Photoexcitation in the Spin-Crossover Compound $[Fe(pic)_3]Cl_2 \cdot EtOH$ (pic = 2-Picolylamine)

Cristian Enachescu,[†] Ueli Oetliker, and Andreas Hauser*

Département de Chimie Physique, Université de Genève, 30 quai Ernest-Ansermet, CH-1211 Genève, Switzerland

Received: March 20, 2002

$[Fe(pic)_3]Cl_2 \cdot EtOH$ (pic = 2-picolylamine) is a spin-crossover compound that can be converted from the low-spin state to the high-spin state at temperatures below the thermal transition temperature by way of light irradiation in the visible part of the electromagnetic spectrum. For this compound, the question regarding the quantum efficiency of this photoconversion process and its possible dependence on irradiation intensity gave rise to some controversy. The experimental results presented in this paper demonstrate that the quantum efficiency of the photoconversion at 11 K is on the order of unity, with no noticeable dependence on irradiation intensity. It does, however, depend to some extent on the fraction of complexes already converted to the high-spin state.

1. Introduction

$[Fe(pic)_3]Cl_2 \cdot EtOH$ (pic = 2-picolylamine) is a well-known compound belonging to the class of so-called spin-crossover compounds.[1] Because of cooperative effects of elastic origin, its thermal spin transition from the diamagnetic $^1A_1(t_{2g}^6)$ low-spin state, which is thermodynamically stable at low temperatures, to the paramagnetic $^5T_2(t_{2g}^4e_g^2)$ high-spin state, which becomes the thermodynamically stable state at elevated temperature, is comparatively abrupt. For $[Fe(pic)_3]Cl_2 \cdot EtOH$, the actual spin transition temperature, that is, the temperature at which half the complexes are in the high-spin state, is ∼118 K. An intriguing feature of the thermal transition curve is the step of ∼7 K,[2] despite the fact that all complexes are crystallographically equivalent. Kohlhaas et al.[3] explained this feature by taking into account short-range correlations with a nonrandom distribution of high-spin and low-spin complexes within the temperature interval of the step that results from specific nearest-neighbor interactions.

The two states in question not only have distinct magnetic properties but also have quite different optical properties. In the high-spin state, $[Fe(pic)_3]Cl_2 \cdot EtOH$ is yellow, with a comparatively weak absorption band centered at 830 nm corresponding to the spin-allowed ligand-field transition $^5T_2 \rightarrow {}^5E$. In the low-spin state, it is red because of an intense metal−ligand charge-transfer (MLCT) band that dominates the spectrum in the visible region.[4] Furthermore, the metal−ligand bond length as well as the volume of the molecules is greater in the high-spin state than in the low-spin state. On average, $\Delta r_{HL} = r_{HS} - r_{LS}$ is ∼0.18 Å,[5] and the corresponding volume difference ΔV_{HL}, corrected for thermal contraction, is ∼9 Å^3.[6]

In spin-crossover compounds, the high-spin state can also be populated quantitatively as a metastable state below the thermal transition temperature by irradiating into either ligand-field or MLCT absorption bands of the low-spin species. This is the so-called light-induced excited spin state trapping (LIESST) effect,[4] in which, according to Scheme 1, an extremely rapid[7] double intersystem crossing step takes the complex from the initially excited state to the high-spin state. At sufficiently low temperatures, the complex is trapped in the high-spin state as a result of the energy barrier due to the large bond-length difference between the two states. For $[Fe(pic)_3]Cl_2 \cdot EtOH$, at temperatures below 10 K, the lifetime of the metastable state is longer than 20 000 s. It decreases to several hundreds of seconds at 50 K.[8] Rather than being single-exponential, the experimental high-spin → low-spin relaxation curves have a sigmoidal shape. This observation can be explained by the above-mentioned cooperative effects, which result in a self-acceleration of the relaxation process.[9] As for the thermal spin transition, in the case of $[Fe(pic)_3]Cl_2 \cdot EtOH$, specific nearest-neighbor interactions and the build-up of a nonrandom distribution of high-spin and low-spin complexes during the relaxation process have to be taken into account.[8]

SCHEME 1. Ligand-Field States of Iron(II) and the Mechanism of Light-Induced Excited Spin State Trapping[a]

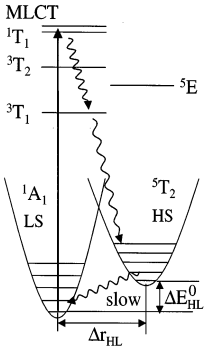

[a] Adapted from ref 1.

In a recent publication, Ogawa et al.[10] studied the photoconversion in the title compound. They suggest that at temperatures of 10 K or below, the quantum efficiency of the photoconversion from the low-spin to the high-spin state depends on the excitation light intensity, and they report values for the quantum efficiency of this process, that is, the number of iron complexes converted per absorbed photon, of up to 34. This value is

* Corresponding author. E-mail: andreas.hauser@chiphy.unige.ch.
[†] On leave from Al. I. Cuza University, Iasi, 6600, Romania.

10.1021/jp020765o CCC: $22.00
Published on Web 08/22/2002

different from the value of approximately unity reported for another typical spin-crossover compound, namely, $[Fe(ptz)_6](BF_4)_2$ (ptz = 1-propyltetrazole),[11] that shows relaxation behavior that is quite similar to that of the title compound. Our independent determination of the quantum efficiency and its dependency on temperature as well as on light intensity, presented in the following discussion, does not confirm the observations reported by Ogawa et al.[10]

2. Experimental Section

A single crystal of $[Fe(pic)_3]Cl_2 \cdot EtOH$, grown as described in ref 12 using a temperature-gradient method, with a thickness of 60 μm and a diameter of ~300 μm was mounted so as to cover a small aperture in a copper sample holder entirely. The sample holder, in turn, was inserted into a closed-cycle cryostat (Oxford Instruments CCC1204) capable of achieving sample temperatures down to 11 K, with the sample sitting in 1 bar of He exchange gas for efficient cooling. This crystal had a maximum absorbance A of ~0.1 (ϵ_{830} = 10 L mol^{-1} cm^{-1}) ($A = \log(I_0/I)$) at 830 nm for the $^5T_2 \rightarrow {}^5E$ ligand-field band of the thermally populated high-spin state at room temperature as well as of the light-induced high-spin state at 11 K.[4] Irradiation experiments at 11 K were performed with the 647 and 676-nm lines of a Kr^+ laser, with intensities I ranging from 0.02 to 7.2 mW/mm^2, corresponding to a photon flux at the sample Φ of 6.5×10^{15} to 2.5×10^{18} s^{-1} cm^{-2}. Both laser lines are in the tail of the intense MLCT band of the low-spin species and at wavelengths where the high-spin species does not absorb. The absorbance of the crystal in the low-spin state is ~0.12 (ϵ_{647} = 12 L mol^{-1} cm^{-1}, $\sigma = 4.6 \times 10^{-20}$ cm^2) at 647 nm and ~0.06 at 676 nm. These rather low values of the absorbance ensure that concentration gradients inside the crystal during photoconversion are minimal and that the crystal survives the photoconversion process without fracturing. Indeed, irradiation at shorter wavelengths, that is, further into the intense MLCT band, creates strong concentration gradients that lead to the disintegration of the crystal into a microcrystalline powder.[8] It is equally important to minimize transverse intensity gradients across the sample. To this end, the laser beam was expanded to ~2.5 mm with a telescope. Care was taken to place the crystal of 0.3-mm diameter in the center of this spot. The irradiation intensity (in mW/mm^2) falling onto the crystal was determined by placing a pinhole of a precisely known diameter of 0.5 mm at the position of the sample and measuring the intensity of the light passing through the pinhole with a calibrated power meter (Coherent Field-Master). A correction for losses due to reflection from the cryostat windows and from the crystal face itself was taken into account.

The fraction of complexes in the high-spin state, γ_{HS}, as a function of irradiation time for the photoconversion as well as for the subsequent high-spin → low-spin relaxation in the dark was determined from the relative intensity of the $^5T_2 \rightarrow {}^5E$ ligand-field band as obtained from full absorption spectra recorded between 500 and 1050 nm at appropriate time intervals. To this end, we used a home-built spectrometer equipped with a CCD camera and an appropriate arrangement of alternating shutters to (a) protect the camera from the laser light during the 100 ms required to record a spectrum and (b) minimize the amount of light from the 50-W tungsten halogen source used to record the spectrum. In addition, the sensitivity of the CCD camera allowed a reduction of the intensity of the latter to 0.1% of the full intensity with a neutral density filter. With less than 0.1 μW/mm^2, the average irradiation from the tungsten halogen lamp is thus truly negligible.

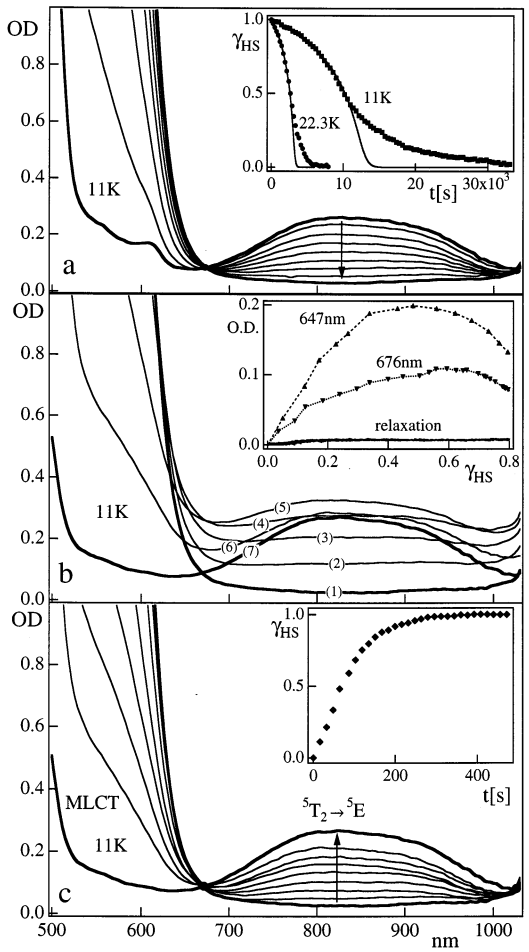

Figure 1. Absorption spectra of $[Fe(pic)_3]Cl_2 \cdot EtOH$ at 11 K in the region of the $^5T_2 \rightarrow {}^5E$ transition: (a) Spectra recorded at intervals of 600 s following complete photoconversion to the high-spin state. Inset: high-spin → low-spin relaxation curves at 11 and 22.3 K; (●) experimental points, (—) fit with mean-field model for $\gamma_{HS} > 0.5$. (b) Uncorrected spectra recorded at intervals of 60 s during continuous excitation at 647 nm, I = 1.6 mW/mm^2. Curves are numbered in chronological order. Inset: baseline shifts due to diffuse scattering for irradiation at 647 and 676 nm. (c) Spectra from Figure 1b corrected for the baseline shift. Inset: corresponding excitation curve at 11 K.

A warning: $[Fe(pic)_3]Cl_2 \cdot EtOH$ is extremely hygroscopic and air sensitive. In the laboratory atmosphere, small crystals turn from yellow to brown quickly. Indeed, they develop brown spots on the surface within minutes. Such sample deterioration is, of course, detrimental to the experiment. Thus, crystals were routinely handled in a glovebox under an inert atmosphere, and the transfer time to the cryostat was minimized. Once inside the cryostat under a helium atmosphere, they are safe from oxidation.

3. Results and Discussion

3.1. Characterization of the Absorption Spectra. Figure 1a presents the evolution of the absorption spectrum of $[Fe(pic)_3]Cl_2 \cdot EtOH$ during the high-spin → low-spin relaxation at 11 K following complete photoconversion with irradiation at 647 nm. Two isosbestic points are clearly discernible: one at ~685 nm and the other one toward the upper limit of the registered spectra, that is, at ~1030 nm. As mentioned above, the band centered at 830 nm corresponds to the spin-allowed ligand-field transition $^5T_2 \rightarrow {}^5E$ of the high-spin species. From its relative intensity as a function of time, the relaxation curve for the high-spin → low-spin relaxation at 11 K shown in the

inset of Figure 1a can be extracted. The inset also includes the relaxation curve recorded at 22.3 K. Both curves are in full agreement with the previously published relaxation curves of Romstedt et al.[8] The sigmoidal, self-accelerated shape is typical for the high-spin → low-spin relaxation in neat spin-crossover compounds and is due to cooperative effects.[9,13] In the case of the title compound, the relaxation curves follow the prediction of a mean-field approach only down to a value of the high-spin fraction of ~0.5. Below this value, there are strong deviations from the mean-field behavior due to specific nearest-neighbor interactions [3] and the build-up of nonrandom distributions of high-spin and low-spin complexes during the relaxation process.[8]

Figure 1b shows the evolution of the absorption spectrum of $[Fe(pic)_3]Cl_2 \cdot EtOH$ during continuous excitation at 647 nm and an intensity of 1 mW/mm^2. Because of the diffuse scattering produced by even minimal concentration gradients and occasional jumps due to cracks developing in the crystal, the baseline shifts. This effect is more dramatic at the beginning of the photoconversion, where the concentration gradient builds up, whereas toward the end of the photoconversion, with the concentration gradient disappearing, the baseline actually returns to its initial position. This interpretation is supported by the observation of a significantly larger baseline shift for irradiation at 647 nm with the larger extinction coefficient as compared to irradiation at 673 nm. The inset of Figure 1b shows the baseline shifts for the two irradiation wavelengths. In fact, the two isosbestic points observed during relaxation in the dark can be used to correct for the baseline shifts in the absorption spectra obtained during irradiation. The resulting true evolution of the absorption spectrum of $[Fe(pic)_3]Cl_2 \cdot EtOH$ under continuous irradiation at 647 nm and an intensity of 1 mW/mm^2 is shown in Figure 1c. From this series of spectra, the high-spin fraction, γ_{HS}, can be extracted as a function of irradiation time. The inset shows the corresponding excitation curve.

3.2. Excitation Curves and the Quantum Efficiency of LIESST. Figure 2a and b shows the excitation curves of $[Fe(pic)_3]Cl_2 \cdot EtOH$ at 11 K for irradiation at 647 nm and intensities between 0.02 and 7.2 mW/mm^2 as obtained by the above procedure. For the highest irradiation intensity of 7.2 mW/mm^2, the photoconversion was complete within less than 30 s, that is, within the same total time as that observed by Ogawa et al.[10] at their highest irradiation intensity. For a quantitative evaluation of these data, it is preferable to plot the high-spin fraction, γ_{HS}, as a function of the product of irradiation time and intensity, *It* (mJ/mm^2), as shown in Figure 3a. In this representation, all curves with irradiation intensities of $I > 0.24$ mW/mm^2 are superimposable within experimental accuracy. For such intensities, the quantitative excitation to $\gamma_{HS} = 1$ is achieved in less than 10^3 s, that is, much faster than the high-spin → low-spin relaxation at 11 K. For $I > 0.24$ mW/mm^2, the latter is negligible. Thus, it can be concluded that the quantum efficiency, η, for the photoconversion does **not** depend upon irradiation intensity. In fact, it is straightforward to extract η from these curves using the differential equation for the build-up of the high-spin state in the case of negligible relaxation

$$d\gamma_{HS}/dt = \eta k_{ex}(1 - \gamma_{HS}) \quad (1)$$

where

$$k_{ex} = \sigma\Phi = 1.5 \times 10^{-2} I\ (s^{-1}) \quad (2)$$

is the rate constant for the primary excitation, σ and Φ are the absorption cross section at the irradiation wavelength and the photon flux, respectively, and I is the irradiation intensity in mW/mm^2. The factor of 1.5×10^{-2} corresponds to an irradiation wavelength of 647 nm and an absorption cross section of $\sigma = 4.6 \times 10^{-20}$ cm^2 ($\epsilon_{647} = 12$ L mol^{-1} cm^{-1}). With $It \approx 80$ mJ/mm^2 at $\gamma_{HS} = 0.64$, η must be approximately unity. However, inspection of the excitation curves of Figure 3 shows that the photoconversion is not exactly single-exponential and therefore that η **does** depend to some extent on the actual high-spin fraction γ_{HS}. This is not surprising because intersystem crossing rate constants are known to be influenced by cooperative effects in spin-crossover systems.[8,14] Indeed, similar behavior has previously been observed for other spin-crossover compounds.[14] η as a function of γ_{HS} can be extracted from the experimental curves by numerical differentiation according to eq 1. Figure 4 shows η as function of γ_{HS} obtained from the ensemble of curves with $I > 0.24$ mW/mm^2. η starts at a value of around 0.5 at the beginning of the irradiation and increases somewhat with increasing values of γ_{HS}. Within experimental accuracy, it does not significantly exceed the value of unity, that is, per absorbed photon only one complex is converted to the metastable high-spin state.

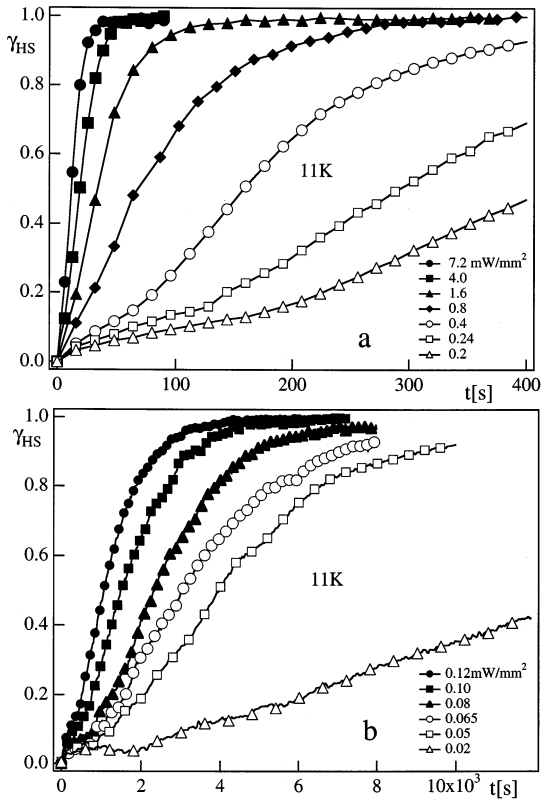

Figure 2. Excitation curves for $[Fe(pic)_3]Cl_2 \cdot EtOH$ at 11 K. Irradiation at 647 nm with intensities varying from 0.02 to 7.2 mW/mm^2.

For values of $I < 0.24$ mW/mm^2, the excitation is not sufficiently fast to overcome the nonzero high-spin → low-spin relaxation due to low-temperature tunneling. Thus, for $I = 0.02$ mW/mm^2, the photoconversion curve levels off at a steady-state value of γ_{HS} that is well below unity. At still lower values of I, the steady-state high-spin fraction obtained after very long irradiation times becomes smaller and smaller. The increasingly sigmoidal shape of the curves as the irradiation intensity is lowered can be understood on the basis of the self-accelerating character of the high-spin → low-spin relaxation due to the above-mentioned cooperative effects.[8,15] It can be modeled on the basis of the differential equation that takes into account the

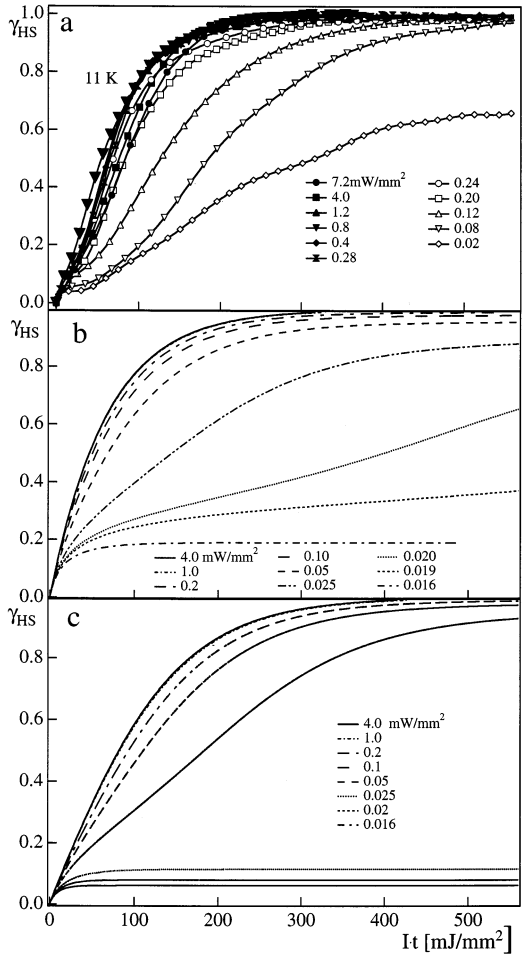

Figure 3. (a) Excitation curves for $[Fe(pic)_3]Cl_2 \cdot EtOH$ at 11 K for irradiation at 647 nm from Figure 2a plotted against the irradiation energy It (mJ/mm^2). (b) Simulated excitation curves calculated using a value of 12 L mol^{-1} cm^{-1} for the extinction coefficient at 647 nm and an average quantum efficiency of 0.8. (c) Simulated excitation curves using the dependence of the quantum efficiency on γ_{HS} as determined experimentally.

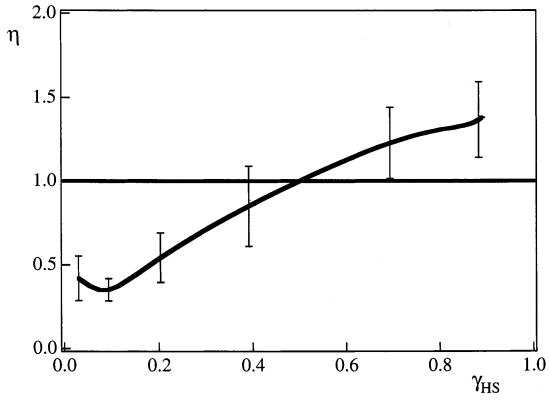

Figure 4. Quantum efficiency η of LIESST for $[Fe(pic)_3]Cl_2 \cdot EtOH$ at 11 K and irradiation at 647 nm as a function of γ_{HS}.

competition between the photoconversion and the relaxation according to[14]

$$\frac{d\gamma_{HS}}{dt} = \eta k_{ex}(1 - \gamma_{HS}) - k_{HL}\gamma_{HS} \qquad (3)$$

in which k_{HL} is a function of the high-spin fraction γ_{HS}. In the mean-field approximation, this function takes the form of an

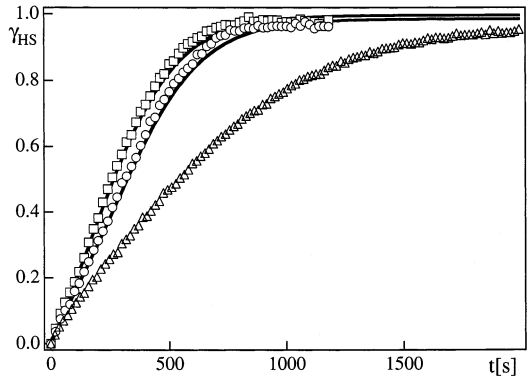

Figure 5. Excitation curves for $[Fe(pic)_3]Cl_2 \cdot EtOH$ at 11 K (□) and 22.3 K (○) for irradiation at 647 nm and at 11 K for irradiation at 676 nm (Δ). Drawn lines: calculated curves using the parameters as described in the text. Irradiation intensity at both wavelengths: 0.25 mW/mm^2.

exponential dependence according to ref 9:

$$k_{HL} = k_{HL}(\gamma_{HS} = 1) \exp[\alpha(1 - \gamma_{HS})] \qquad (4)$$

Despite the fact that this form of $k_{HL}(\gamma_{HS})$ describes only the relaxation curves for $\gamma_{HS} > 0.5$ (see Figure 1a), it is the correct form to take for the present case of continuous irradiation. As Romstedt et al.[8] have shown, under irradiation, the title compound behaves as predicted by the mean-field approach for all values of γ_{HS} because the irradiation actually destroys correlations. For the title compound at 11 K, the exponential self-acceleration factor $\alpha \approx 4.5$, and the initial rate constant $k_{HL}(\gamma_{HS} = 1) \approx 2 \times 10^{-5}$ s^{-1}. With these values, the numerical solution of the above differential equation gives the theoretical excitation curves shown in Figure 3. For the curves of Figure 3b, a constant quantum efficiency of 0.8 was assumed; for the curves of Figure 3c, a linear variation of the quantum efficiency according to the experimental curve of Figure 4 was used. The key features of the observed curves, namely, a threshold value for the irradiation intensity above which full photoconversion occurs and an incubation period for lower values of the intensity with a plateau before the curve reaches its final steady-state value of γ_{HS}, are nicely reproduced by the simulations.[16] In particular, for the second case, very good agreement between the sigmoidal shape of the experimental curves and the simulated curves is obtained.

Figure 5 compares the excitation curves at 11 and 22.3 K for irradiation at 647 nm and a light intensity of 0.4 mW/mm^2. The difference between the excitation curves recorded at 11 and 22.3 K, could, in principle, be due to either a faster relaxation or a smaller quantum efficiency for LIESST at 22.3 K. It is comparatively straightforward to show that it is basically due to the former. From the relaxation curves at 11 and 22.3 K shown in the inset of Figure 1a, both the above-mentioned values of 2×10^{-5} s^{-1} for $k_{HL}(\gamma_{HS} = 1)$ and 4.5 for α at 11 K as well as values of 1×10^{-4} s^{-1} and approximately 4.5 for α at 22.3 K can be extracted. In Figure 5, the excitation curves calculated by numerical integration of differential eq 3, the dependence of $k_{HL}(\gamma_{HS})$ according to eq 4 with the above sets of parameters for the curves, and a temperature-independent quantum efficiency according to Figure 4 are included. The good agreement between experimental and calculated curves allows us to conclude that the quantum efficiency of LIESST is indeed temperature-independent.

Figure 5 also includes the excitation curve at 11 K that was obtained for irradiation at 676 nm and the same light intensity

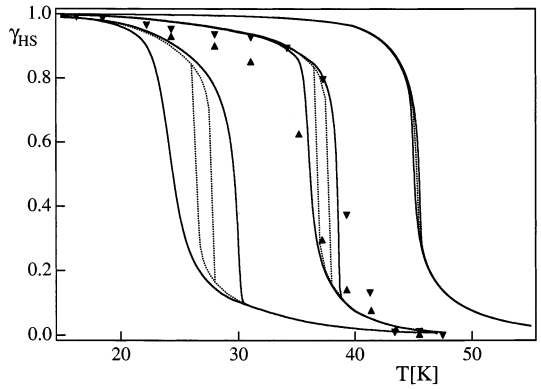

Figure 6. Light-induced hysteresis curves obtained by scanning the temperature under continuous irradiation at 647 nm with an intensity of 0.8 mW/mm^2. Experimental points: scan speed 3 K/h increasing (▼) and decreasing (▲). Drawn lines: calculated curves with $I = 0.2$, 0.8, and 3.2 mW/mm^2 and a scan speed of 3 K/h. Broken lines: calculated curves with the same irradiation intensities but under steady-state conditions (for details, see text).

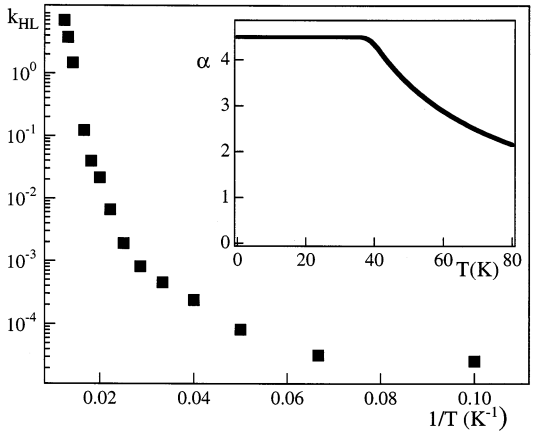

Figure 7. High-spin → low-spin relaxation rate constant plotted as $\ln[k_{HL}(T)]$ versus $1/T$ for $[Fe(pic)_3]^{2+}$ doped into $[Zn(pic)_3]Cl_2 \cdot EtOH$ from ref 19. Inset: acceleration factor α as a function of T according to ref 13.

as for the irradiation at 647 nm. Of course, irradiation at 676 nm results in a slower population of the high-spin state than irradiation at 647 nm, but this is simply due to the fact that at 676 nm the absorption cross section is roughly half as large as that at 647 nm. The effective quantum efficiency is the same for the two irradiation wavelengths.

3.3. Light-Induced Thermal Hysteresis. Some time ago, it was realized that a substantial high-spin fraction can be maintained at temperatures above the temperature where thermal relaxation normally occurs by way of continuous irradiation in a steady-state-type situation. The same cooperative effects that result in the sigmoidal relaxation curves can also result in a so-called light-induced thermal hysteresis,[17,18] provided the interaction is sufficiently large. Figure 6 presents the light-induced thermal hysteresis observed for $[Fe(pic)_3]Cl_2 \cdot EtOH$. The experimental curves were obtained by irradiating the sample with a continuous intensity of 0.8 mW/mm^2 and by varying the temperature at an average speed of ∼3 K/h, first from 11 to 47 K and then by reversing the temperature scan back to 10 K. The observed hysteresis has a width of ∼4 K. To determine whether the hysteresis is real or the result of too fast a temperature scan, a simulation of the experimental curves was performed by way of a numerical integration of differential eq 3. The key to a successful simulation is the precise knowledge of $k_{HL}(\gamma_{HS} = 1)$ and the acceleration factor α of eq 4 as functions of temperature. The actual values of the two parameters are not available as functions of temperature. $k_{HL}(\gamma_{HS} = 1)$ may be taken from the literature as the rate constant of the single-exponential high-spin → low-spin relaxation of $[Fe(pic)_3]^{2+}$ doped into the isostructural host $[Zn(pic)_3]Cl_2 \cdot EtOH$.[19] The zinc host essentially simulates an inert high-spin lattice.[20] In Figure 7, the corresponding rate constant is plotted as $\ln[k_{HL}(T)]$ versus $1/T$. The initial rate constants at 11 and 22.3 K as derived from the relaxation curves in the inset of Figure 1 confirm this. In the mean-field approximation, the acceleration factor α is known to be constant between 10 and ∼40 K. Above 40 K, α decreases as Γ/k_BT,[13] where Γ is the interaction constant of the thermal spin transition in the mean-field approximation. As mentioned above, for $[Fe(pic)_3]Cl_2 \cdot EtOH$, the low-temperature value $\alpha \approx 4.5$, and from the thermal spin transition, $\Gamma \approx 175$ cm^{-1}.[3,20] Thus, the dependence of α included in the inset of Figure 7 is appropriate for simulating light-induced thermal hysteresis curves. The results of such a simulation for three different irradiation intensities, namely, the intensity actually used in the experiment ($I = 0.8$ mW/mm^2), one at a quarter of this value and one at four times this value, are included in Figure 6. In addition, the simulations were carried out for the actual temperature scan rate of ∼3 K/h as well as for a hypothetical infinitely small scan rate. The curves calculated using the intensity as well as the temperature scan rate of the experiment are in good agreement with the experimental curves. In particular, the actual temperature of ∼38 K, up to which the system can be maintained in the high-spin state at the chosen irradiation intensity, and the associated width of the hysteresis of ∼4 K are nicely reproduced. Thus, it may be concluded that the assumptions of a temperature-independent quantum efficiency at least up to 40 K and an approximately constant value of $\alpha \approx 4.5$ are indeed justified. However, it must be noted that despite the slow temperature variation the hysteresis of ∼4 K is not entirely due to the cooperative effects. The hysteresis predicted for an infinitely slow variation of the temperature with a true steady-state-type situation at all times is considerably smaller. To determine the true width of the light-induced hysteresis, the temperature scan rate would have to be less than 0.5 K/h under the irradiation intensity of the actual experiment.

The simulations with the smaller and larger light intensities as compared to the intensity of the actual experiment show that the temperature up to which the high-spin state can be maintained varies with intensity. More importantly, the width of the light-induced hysteresis varies. At low irradiation intensities and thus at low temperatures, it is larger, and the effect of a noninfinitely slow temperature variation on the apparent hysteresis becomes quite dramatic. At high irradiation intensities and the associated higher temperatures, the value of α drops to below the critical value for which light-induced hysteresis is to be expected, and even at a scan rate of 3 K/h, the apparent hysteresis becomes quite small.

Considering the fact that the calculated curves of the light-induced thermal hysteresis are not the result of a fitting procedure but are based on values of the various parameters as determined from independent experiments, the agreement between the experimental and calculated curves is excellent. There are, however, some systematic deviations. These could have their origin in the limits of the mean-field approach, that is, in the build-up of correlations. This would be expected to be especially important for the temperature scan from high to low temperatures, for which the largest deviations from the calculated curves are observed. However, it must be remembered that the experiment under consideration is extremely demanding

in terms of the long-term stability of all experimental parameters such as light intensity, mechanical stability, and crystal quality. Despite great efforts to minimize intensity and thus concentration gradients, these cannot be entirely eliminated. Small longitudinal and transversal gradients as well as deteriorating crystal quality may influence the experimental curves to an extent that is difficult to model.

4. Conclusions

On the basis of previous publications on the thermal spin transition[2,3,21] as well as on the photophysical properties[8] of $[Fe(pic)_3]Cl_2 \cdot EtOH$, the results presented in this article lead to a quantitative, comprehensive, and consistent understanding of the various aspects of light-induced excited spin state trapping in this compound. In conclusion, all observations can be interpreted on the basis of comparatively simple and well-established theoretical concepts. In $[Fe(pic)_3]Cl_2 \cdot EtOH$, as in other spin-crossover systems, the quantum efficiency for the light-induced population of the metastable high-spin state at 10 K is on the order of unity. It does not depend on the irradiation intensity, and it does not depend noticeably upon temperature in the temperature interval between 10 and 50 K. However, as a result of cooperative effects, it does depend to some extent on the high-spin fraction. The light-induced hysteresis curves can be quantitatively modeled by explicitly taking into account the speed of the temperature variation and the correct variation both of the relaxation constant at $\gamma_{HS} = 1$ and the corresponding acceleration factor α.

We cannot in any way confirm the extraordinary quantum efficiency of up to 34 for the high irradiation intensities proposed by Ogawa et al.[10] In fact, from a mechanistic as well as from a thermodynamic point of view, such quantum efficiency would be difficult to explain. In these molecular crystals, electronic interactions, especially in the absence of bridging ligands, are negligible. The initial excitation is thus localized on a single complex. This complex relaxes to the high-spin state, whereby it releases surplus energy in the form of vibrations. The fact that the high-spin state is trapped within picoseconds[7] indicates that this vibrational energy is efficiently dissipated into the surroundings. That this vibrational energy should be picked up by the surrounding complexes and reconverted at 100% efficiency into highly ordered electronic energy seems highly improbable; in fact, it seems to violate the second law of thermodynamics. Of course, it may be argued that at a high enough excitation intensity a given fraction of high-spin complexes induces major crystallographic rearrangements, that is, a crystallographic phase transition, as is the case for the thermal spin transition in the well-studied spin-crossover compound $[Fe(ptz)_6](BF_4)_2$,[15] whereby the effective energy difference between the high-spin and the low-spin states is lowered to such an extent that the high-spin state becomes the quantum mechanical ground state. In this case, an additional thermodynamic driving force for the conversion to the high-spin state could have interesting effects. However, such a scenario is unlikely because one would then expect that after the system entered the high-spin state it would actually stay in the high-spin state indefinitely at low temperatures, which it does not.

Acknowledgment. We thank our colleague and friend Hartmut Spiering for helpful discussions. This work was financially supported by the Swiss Federal Office for Research and Education, grant no. 970559 within the European TMR project ERB-EMRX-CT98-0199, and by the Swiss National Science Foundation.

References and Notes

(1) Gütlich, P.; Hauser, A.; Spiering, H. *Angew. Chem., Int. Ed. Engl.* **1994**, *33*, 2024.
(2) Köppen, H.; Müller, E. W.; Köhler, C. P.; Spiering, H.; Meissner, E.; Gütlich, P. *Chem. Phys. Lett.* **1982**, *91*, 348.
(3) Kohlhaas, Th.; Spiering, H.; Gütlich, P. *Z. Phys. B: Condens. Matter* **1997**, *102*, 455.
(4) Decurtins, S.; Gütlich, P.; Hasselbach, K. M.; Hauser, A.; Spiering, H. *Inorg. Chem.* **1985**, *24*, 2174.
(5) Mikami, M.; Konno, M.; Saito, Y. *Acta Crystallogr., Sect. B* **1982**, *38*, 452.
(6) Wiehl, L.; Kiel, G.; Köhler, C. P.; Spiering, H.; Gütlich, P. *Inorg. Chem.* **1986**, *25*, 1565.
(7) McCusker, J. K.; Walda, K. N.; Dunn, R. C.; Simon, J. D.; Magde, D.; Hendrickson, D. N. *J. Am. Chem. Soc.* **1992**, *114*, 6919.
(8) Romstedt, H.; Hauser, A.; Spiering, H. *J. Phys. Chem. Solids* **1998**, *59*, 265.
(9) Hauser, A. *Chem. Phys. Lett.* **1992**, *192*, 65.
(10) Ogawa, Y.; Koshihara, S.; Koshino, K.; Ogawa, T.; Urano, C.; Takagi, H. *Phys. Rev. Lett.* **2000**, *84*, 3181.
(11) Hauser, A. *J. Chem. Phys.* **1991**, *94*, 2741.
(12) Sorai, M.; Ensling, J.; Gütlich, P. *Inorg. Chem.* **1976**, *18*, 199.
(13) Hauser, A.; Jeftic, J.; Romstedt, H.; Hinek, R.; Spiering, H. *Coord. Chem. Rev.* **1999**, *190*−*192*, 471.
(14) Enachescu, C.; Constant-Machado, H.; Boukheddaden, K.; Codjovi, E.; Linares, J.; Varret, F. *J. Phys. Chem. Solids* **2001**, *62*, 1409.
(15) Jeftic, J.; Hauser, A. *J. Phys. Chem. B* **1997**, *101*, 10262.
(16) Koshino, K.; Ogawa, T. *J. Lumin.* **2000**, *87*−*89*, 642.
(17) Desaix, A.; Roubeau, O.; Jeftic, J.; Haasnoot, J. G.; Boukheddaden, K.; Codjovi, E.; Linares, J.; Nogues, M.; Varret, F. *Eur. Phys. J. B* **1998**, *6*, 183.
(18) Letard, J.-F.; Guionneau, P.; Rabardel, L.; Howard, J. A. K.; Goeta, A. E.; Chasseau, D.; Kahn, O. *Inorg. Chem.* **1998**, *37*, 4432.
(19) Vef, A.; Manthe, U.; Gütlich, P.; Hauser, A. *J. Chem. Phys.* **1994**, *101*, 9326.
(20) Jakobi, R.; Spiering, H.; Gütlich, P. *J. Phys. Chem. Solids* **1992**, *68*, 267.
(21) Spiering, H.; Kohlhaas, Th.; Romstedt, H.; Hauser, A.; Bruns-Yilmas, C.; Kusz, J.; Gütlich, P. *Coord. Chem. Rev.* **1999**, *190*−*192*, 629.